Modeling momentum and scalar transport in a wall-bounded turbulent flow

Theresa Saxton-Fox

Department of Mechanical and Civil Engineering
California Institute of Technology
1200 E California Blvd. Pasadena, CA 91125. USA.
tsaxtonf@caltech.edu

Beverley McKeon

Graduate Aerospace Laboratories
California Institute of Technology
1200 E California Blvd. Pasadena, CA 91125. USA.
mckeon@caltech.edu

ABSTRACT

A mildly-heated turbulent boundary layer was studied to characterize the relationship between velocity structures and the scalar field. Particle image velocimetry (PIV) and a Malley probe (Malley *et al.*, 1992) were used to simultaneously measure the velocity field and the streamwise gradients of the scalar field (Gordeyev *et al.*, 2014) respectively. Two distinct velocity scales were identified to be correlated to scalar mixing by conditionally averaging the velocity field on the existence of a scalar gradient. Resolvent analysis was used to create simple models of these velocity scales (McKeon & Sharma, 2010) and to probe their interaction. Using a combination of structural conditional averaging and conditional averaging on the scalar gradient, significant interaction was observed between the two scales of interest, with behavior consistent with the general scale interaction described by amplitude modulation (Hutchins & Marusic, 2007). The study constructed a model of the velocity field that was correlated to streamwise scalar gradients in the outer boundary layer.

INTRODUCTION

The relationship between the scalar field and the velocity field in wall-bounded turbulent flows has been studied for decades. Chen & Blackwelder (1978) used the temperature field of a turbulent boundary layer developing over a heated wall to identify sharp shear layers on the backs of large-scale bulges. These sharp shear layers were found to spatially coincide with sharp changes in the temperature field, suggesting significant correlation between the streamwise velocity field and the scalar field in the outer boundary layer. For flows with Prandtl number near unity, the velocity and scalar fields have been statistically related using the Strong Reynolds Analogy and extended Strong Reynolds Analogy, the latter of which has allowed for good estimates of the scalar field in compressible flows with Mach number up to 3 (Wyckham & Smits, 2009; Gordeyev *et al.*, 2014). Instantaneous relationships between the velocity and scalar fields have recently been studied in more detail by Antonia *et al.* (2009). They observed strong similarity between the streamwise velocity field and the scalar field near the wall, which is consistent with usual approximations of their relationship. However, far from the wall, significant differences between the scalar and streamwise velocity fields were observed, even for a flow with Prandtl number near one (0.7) and canonical conditions. In this region of the flow the best match to the scalar field instantaneously and statistically was found to be q where $q^2 \equiv u^2 + v^2 + w^2$ and u, v, and w are the fluctuating streamwise, wall-normal and spanwise velocity fields. Even choosing q as the basis of comparison, the correlation coefficient between instantaneous snapshots of the fluctuating temperature field squared and q^2 was only 0.35, indicating that there are complex relationships between these two fields that are not yet well characterized.

The interaction between scales in the velocity field is also an area of current study. Hutchins & Marusic (2007) demonstrated that very large scale structures in the streamwise velocity field were correlated to a modulation in the strength of small scale velocity structures in the flow. The effect spanned the full height of the boundary layer, but showed different behaviors at different heights. Small scales were shown to be strongest away from the wall in the presence of a negative large scale streamwise velocity feature and strongest near the wall in the presence of a positive large scale streamwise velocity feature (Mathis *et al.*, 2009). This correlation was interpreted as a measure of the phase lag between large and small scales throughout the boundary layer (Jacobi & McKeon, 2013).

This study aimed to improve the understanding of the structural relationships between the scalar and velocity fields in the outer region of turbulent wall-bounded flows. First, conditional averaging techniques were used to identify velocity structures that were correlated to streamwise scalar gradients in a mildly-heated turbulent boundary layer. Two distinct velocity scales were observed, and the interaction of the two scales was investigated using novel conditional averaging and modeling techniques. The individual velocity scales and their interactions were modeled using resolvent analysis, and the possibility of ultimately modeling the scalar field was discussed.

EXPERIMENTAL METHODS

Experiments were carried out in the Merrill wind tunnel at Caltech, an incompressible flow facility with a 0.6 m x 0.6 m text section. A turbulent boundary layer was tripped at the leading edge of a flat plate. Heating elements were embedded in the flat plate over its full span and over a total of 36δ in the streamwise direction, broken into two 18δ sections with a 4δ unheated length between them. The heated portion of the plate started 9δ downstream of the boundary layer trip and ended 6δ before the measurement location. The internal cool layer that developed after the end of the heated section was found to extend up to about 0.1δ in the wall-normal direction at the measurement location. As this paper focuses on the outer region of the boundary layer, this inner cool region is not of interest. Figure 1a shows a schematic of the PIV and Malley probe measurements in the heated turbulent boundary layer, not to scale.

The temperature difference between the free stream and plate was held constant at 20C such that the flow was moderately heated, with no change observed in the statistics of the velocity field from the addition of the scalar. Simultaneous observations of the scalar and velocity fields were conducted, with a Re_τ of 910, Re_θ of 3300, and a Prandtl number of 0.7. The 99% boundary layer thickness was 35 mm.

Velocity measurement

The velocity field was measured using particle image velocimetry (PIV) in the wall-normal streamwise plane. The flow was seeded with an aerosol of bis(2-ethylhexyl)sebacate (DEHS) with a 0.25 μm modal size using the LaVision Aerosol Generator #1108926, and illuminated using a double-pulsed YAG laser. A Photron camera imaged the flow field at a frame rate of 1500 Hz

with a field of view of 1.7 δ x 1.6 δ (60 mm x 55 mm). Velocity vectors were calculated from the images using the DaVis software from Lavision. A double-pass approach was used with window sizes of 32 and then 16 pixels. The final resolution of the vector field was 0.013 δ or 14.5 inner units in both the streamwise and wall-normal coordinates. Statistics of the velocity field were found to agree with data from DeGraaff & Eaton (2000) above a wall-normal height of 0.04δ or 40 inner units. Below that height glare from the wall prevented the accurate measurement of the velocity field.

Scalar measurement

The scalar field was measured using an aero-optic device called a Malley probe (Malley *et al.*, 1992). The Malley probe consists of a laser beam (1 mm diameter) that is passed through a flow before ultimately impinging on a position sensor that measures the beam's centroid position. The final angle of the beam is then deduced from its centroid position, schematically illustrated in figure 1b. The beam angle is found to be time varying when the beam is passed through a variable-density flow, due to a relationship between index of refraction and density (Gordeyev *et al.*, 2014). In air, the index of refraction is in general a function of time and space, $n(x,y,z,t) = 1 + K_{GD}\rho(x,y,z,t)$, where K_{GD} is the Gladstone-Dale constant and ρ is the density field. In this study, the Malley probe is used to study a very low Mach number flow ($M = 0.05$) with heat addition, such that the only source of density fluctuations comes from the heated flat plate (Gordeyev *et al.*, 2015). The beam is passed through the flow in the wall-normal direction and the streamwise angle of the beam is measured. The streamwise beam angle, θ, is a measure of the integral of streamwise gradients in the scalar field. Note that in the schematic in figure 1b the streamwise density gradient is simply represented using a single 'interface' in the density field, illustrated using a dark red inclined line.

$$\sin(\theta(t)) = \sin(\theta_i) + \frac{K_{GD}}{1 + K_G D\rho_a}\int_{\zeta_i}^{\zeta_f}\frac{\partial\rho}{\partial x}\sqrt{\dot{x'^2} + \dot{y'^2} + \dot{z'^2}}d\zeta \quad (1)$$

where θ_i is the incoming angle of the beam relative to the vertical, x', y', z' are the coordinates of the beam in space as a function of the beam path parameterization coordinate ζ, and ρ_a is the ambient air density. Assuming small angles and standard ambient conditions, this can be approximated as

$$\theta(t) \approx K_{GD}\int_{y_i}^{y_f}\frac{\partial\rho}{\partial x}(x_0, y, z_0, t)dy \quad (2)$$

where x_0 and z_0 are the streamwise and spanwise locations of the incoming beam.

MODELING METHODS

The wall-normal coherence of specific velocity scales was modeled using resolvent analysis for a boundary layer geometry with a parallel flow assumption (Jacobi & McKeon, 2011). Resolvent analyses formulate the Navier-Stokes equations as an input-output system where the linear dynamics act as a transfer function between some input and the velocity field. The transfer function is termed the resolvent operator. Fourier transforms were performed in the streamwise, spanwise, and temporal variables to isolate the wall-normal structure of the velocity field as the output of the input-output system. The resolvent operator can be decomposed in a singular value decomposition to determine the right and left singular vectors for each wavenumber triplet (streamwise, spanwise, and temporal). The operator was found to be low rank (McKeon & Sharma, 2010) such that the first left singular vector could be used as an approximation for coherence of the velocity scale. The model for a given scale, defined using its wavenumber triplet, is the first left singular value at that scale with an amplitude set through comparison to PIV data.

IDENTIFYING INDIVIDUAL VELOCITY SCALES

Conditional Averaging

The study aimed to identify structures in the velocity field that were most correlated to scalar mixing. To do this, the Malley probe signal was used as a condition upon which the velocity field was averaged, essentially using the density field as a marker for turbulent structure. The velocity field was conditionally averaged on $\theta < -0.5\sigma$ where σ is the standard deviation of $\theta(t)$, isolating velocity structures that appeared simultaneously with moderately-large negative streamwise gradients of density at any height in the flow. Figure 2a shows the conditionally averaged fluctuating streamwise velocity field, $< u > /U_\infty$, where $<>$ indicates conditional averaging. A feature can be observed that is over 1δ in width. This feature is hypothesized to be the same type of bulge that was observed by Chen & Blackwelder (1978). Figure 2b shows the conditionally averaged wall-normal velocity field $< v > /U_\infty$, where small-scale features are observed (Saxton-Fox *et al.*, 2015). These features are found to have a streamwise length scale of approximately 0.2δ, with a height that spans the entire height of the boundary layer.

That organized structures were observed in the conditionally averaged velocity fields has two implications. The first is that there is some strong relationship between the organization of the scalar field and velocity structures in both the streamwise and wall-normal velocity fields. The second is that the Malley probe signal at a given instant in time is likely dominated by a single event, a localized streamwise density gradient, rather than reflecting an average of multiple events in the flow.

Modeling

Resolvent analysis was used to model the wall-normal coherence of the two scales in figures 2a and b. The feature in the streamwise velocity field was estimated as having a wavelength of 4δ based upon the structure observed in figure 2a, characteristics of bulges from Kovasznay *et al.* (1970), and statistical features of large scale motions described by Monty *et al.* (2009). The spanwise coherence was estimated as 1δ from the work of Kovasznay *et al.* (1970). The second scale was estimated as having a streamwise wavelength of 0.2δ from the structure identified in figure 2b. Its spanwise wavelength was unknown but was estimated as 0.2δ. A convection velocity for both of these structures of $0.8U_\infty$ was selected based upon previous work on the convection velocity of structures that dominate the Malley probe signal in the heated turbulent boundary layer (Saxton-Fox *et al.*, 2015). Figure 3a shows a streamwise – wall-normal cut of the model for the large scale motion observed in the streamwise conditional average, while figure 3b shows a streamwise – wall-normal cut of the model of the wall-normal velocity feature. Note that the wall-normal model in particular is significantly more compact in the wall-normal direction than the conditional averaging result. This discrepancy is explored in further sections.

VELOCITY SCALE INTERACTION

Conditional Averaging

The interaction of the two scales shown in figure 2 was investigated under the hypothesis that, if both scales are correlated to

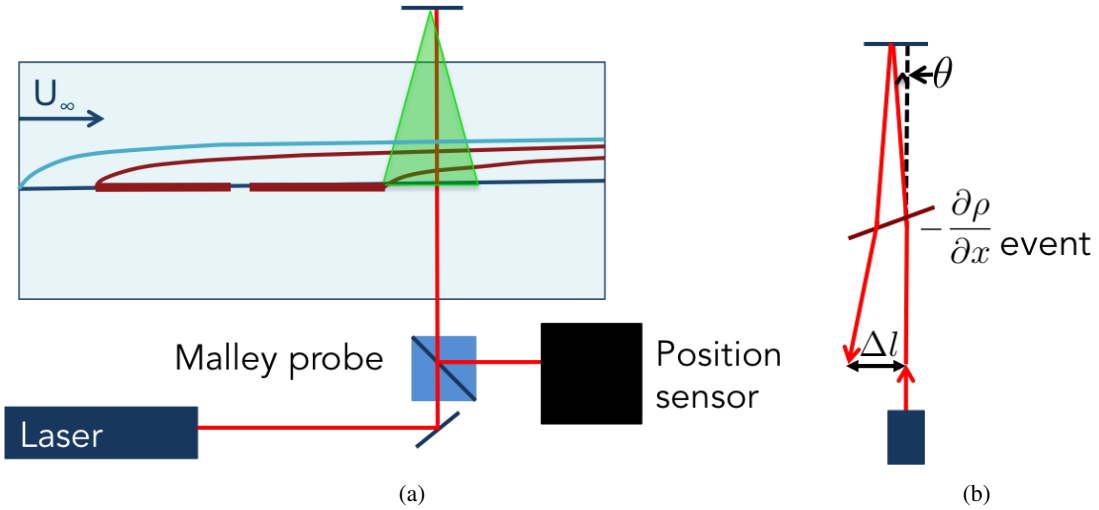

(a) (b)

Figure 1: Schematic of the (a) the PIV and Malley probe simultaneous measurements in a heated, turbulent boundary layer and (b) a simplified representation of the Malley probe optical measurement.

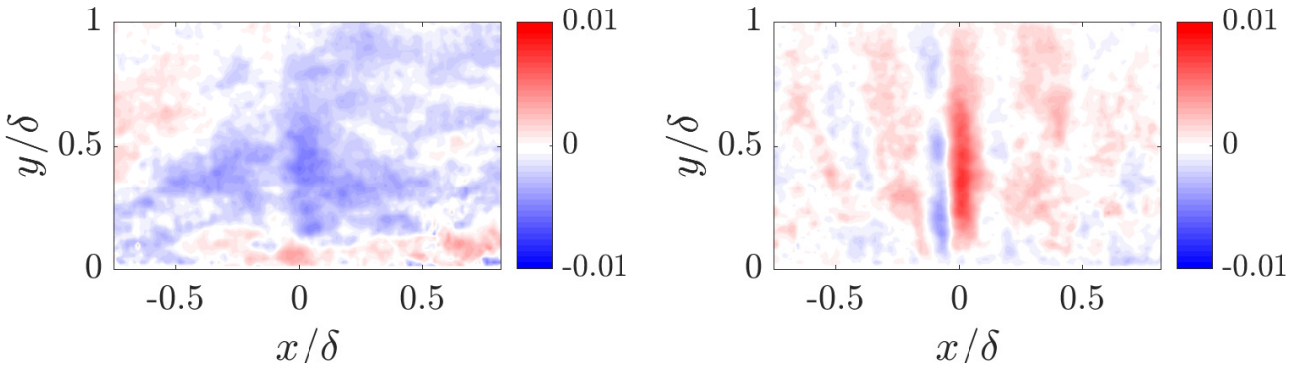

(a) (b)

Figure 2: Conditional averages of (a) the streamwise velocity fluctuations $< u > /U_\infty$ and (b) the wall-normal velocity fluctuations $< v > /U_\infty$ given $\theta < -0.5\sigma$, corresponding to a moderately-large negative streamwise gradient of density along the line $x = 0$.

large streamwise density gradients, perhaps their interaction is relevant to the organization of the scalar field. A modified conditional averaging technique comprised of two unique conditions is used to investigate scale interaction and its relevance to scalar mixing. The first condition was the same as that used to conditionally average to find individual velocity scales: $\theta < -0.5\sigma$. This condition imposed the requirement of a moderately large negative streamwise density gradient. The second condition was that the large scale streamwise structure, modeled in figure 3a, was clearly observable in the instantaneous PIV frame. This condition was achieved using a projection technique. The velocity field was projected onto the resolvent mode and was averaged only if the projection coefficient was above a threshold (in this case, 0.4). Note that because the field of view available in the PIV data was less than the wavelength of the mode, the velocity field was projected onto the mode at eight distinct phases and then stitched together in post-processing.

The wall-normal velocity field was filtered with a Gaussian filter with standard deviation 1δ to obtain the small scale features, v_{ss}. Figure 4 shows a compilation of eight conditionally averaged fields of (a) the streamwise velocity field and (b) the small scale wall-normal velocity field using the modified conditional averaging technique. The black line in figures 4a and b represents an isocontour of the conditionally averaged streamwise velocity field in the laboratory frame $< u > +\bar{U} = 0.8U_\infty$ where $\bar{U}$ is the mean streamwise velocity field. Note that $0.8U_\infty$ is estimated to be the phase speed of both structures and was used to create the models in figures 3a and b.

The coherent regions of wall-normal velocity in figure 4b are observed to appear at different heights relative to the wall as a function of the phase of the large scale. In particular, the height of the coherent regions of wall-normal velocity appears to follow the location of the isocontour of the streamwise velocity field. This specific relationship between the two scales in the flow agrees with the trends between all large and small scales that were identified by Hutchins & Marusic (2007).

Note that compared to the structure in figure 2b, the wall-normal velocity structures in figure 4b are significantly more compact in the wall-normal direction and sit at a particular height in the flow. Their height relative to the large scale structure places them coincident with strong shear layers in the velocity field. The localization of the small scale coherence in v on the strong shear layer suggests that it may be the interaction between a gradient in u and a gradient in v that is ultimately most correlated to strong gradients in the density field. The overlap of the u and v gradients also strengthens the hypothesis that a single strong gradient event is dominating the Malley probe signal, allowing the integral measurement to behave similarly to a point measurement. The large wall-normal extent of the structure observed in figure 2b is hypoth-

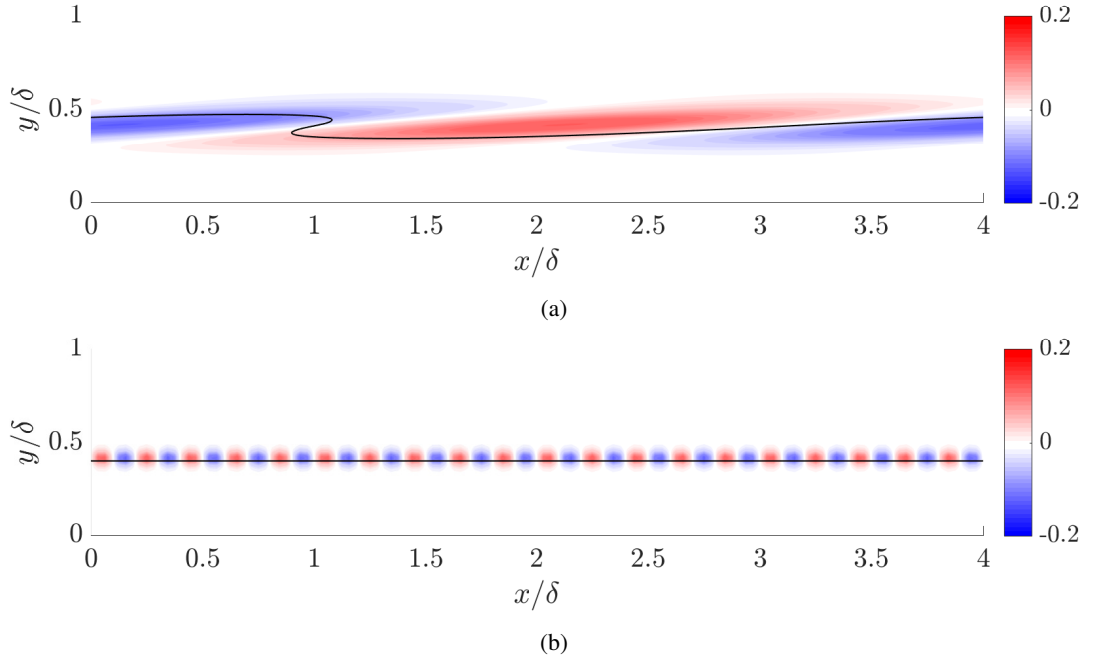

(a)

(b)

Figure 3: Models of (a) the streamwise and (b) the wall-normal velocity structures observed in figure 2, shown in the wall-normal – streamwise plane. Resolvent analysis is used to identify the wall-normal coherence of the models. The black line in (a) indicates $u+\bar{U}=0.8U_\infty$ where u is the streamwise fluctuating velocity field of the resolvent mode, while in (b) it indicates $\bar{U}=0.8U_\infty$.

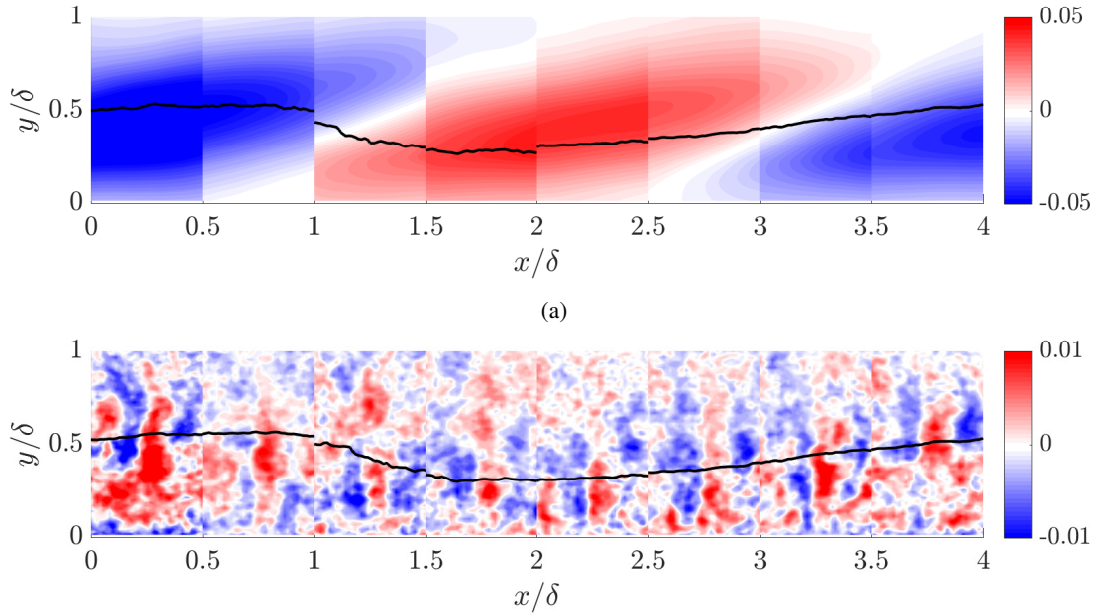

(a)

(b)

Figure 4: Conditional averages of (a) the streamwise velocity field $< u > /U_\infty$ and (b) the small scale wall-normal velocity field $< v_{ss} > /U_\infty$ given two conditions. The first condition is $\theta < -0.5\sigma$ at a particular x location. The second is that the projection of the streamwise velocity field onto the model shown in figure 3a is sufficiently strong, quantified by a projection coefficient larger than 0.4. The projection and conditional averaging are done over eight phases of the resolvent model, as the field of view of the data is less than the streamwise wavelength of the structure. The eight panels are shown stitched together, such that the strong scalar gradients occur at x/δ locations between 0.25 and 3.75 in increments of 0.5. The black line in both (a) and (b) represents $< u > +\bar{U}=0.8U_\infty$.

esized to be the result of averaging the compact structures observed in figure 4b at their different heights in the boundary layer, effectively smearing the small scale in y. Additionally, the compactness of the small scale v coherence suggests that the resolvent model in figure 2b is a reasonable approximation of the instantaneous structure. This resolvent model will be used further in investigating the

observed scale interactions.

Modeling

The scale interaction shown in figure 4b was modeled using multiple resolvent modes and phase information derived from amplitude modulation observations (Mathis *et al.*, 2009; Jacobi & McKeon, 2013). A total of eleven resolvent modes were used, with a total of three values of k_x and k_z. The modes consisted of five 'triads', sets of modes in which two of the wavenumbers sum to the third. All five triads consist of the same large scale, called mode 1, with $k_x = \pi/2$ and $k_z = 2\pi$ (the mode shown in figure 3a). Each triad's mode 2 has spatial wavenumbers $k_x, k_z = 10\pi$ (the same values as figure 3b), and each triad's mode 3 has spatial wavenumbers $k_x = 9.5\pi$ and $k_z = 8\pi$. The distinction between the five triads comes from the temporal wavenumbers, ω, of modes 2 and 3. The phase speed, c, of the mode 2 was set to range from $0.76U_\infty$ to $0.84U_\infty$ in increments of $0.02U_\infty$. This set the temporal wavenumbers of mode 2 through the relation $\omega = ck_x$. The temporal wavenumbers of mode 3 were set such that $\omega_3 = \omega_2 - \omega_1$.

Figure 5b shows the wall-normal velocity field that is the result of the superposition of the ten small scale modes: mode 2 and 3 at each of the five temporal wavenumbers. One observes that mode 2 and mode 3 beat in phase with mode 1, shown for reference in figure 5a. Figure 5b will stay coherent in time because, though the individual small scale modes have differing phase speeds, the sum of mode 2 and mode 3 beat with an envelope that has the same phase speed as mode 1.

The favorable agreement between figure 4b and figure 5b supports the use of figure 5 as a model for the velocity structure that is most correlated to strong streamwise density gradients. This velocity structure is composed of two unique scales with important dynamics in both streamwise and wall-normal velocity components, with interactions that seem to be linked to the scalar field behavior.

DISCUSSION AND CONCLUSIONS

The instantaneous relationship between the scalar field and the velocity field, even in passive scalar transport systems with Prandtl numbers near unity, is rich and complex. This study identifies two distinct scales in the streamwise and wall-normal velocity fields that are correlated to scalar gradients, and identifies a specific scale interaction phenomenon that is related to the scalar transport. A model is proposed to represent the full velocity structure that is most correlated to the streamwise scalar gradient in the outer boundary layer. This velocity structure is composed of the two velocity scales that interact in ways that are consistent with descriptions of amplitude modulation (Hutchins & Marusic, 2007).

The exact form of the scalar field that is correlated to the modeled velocity field has not yet been identified. However, some hypotheses can be made. From the work of Chen & Blackwelder (1978), in flows with Prandtl number near unity strong velocity gradients are known to spatially coincide with strong scalar gradients. Thus, one can expect that the strong shear layer that exists along the isocontour shown in black in figures 4 and 5 coupled with the strong velocity gradient associated with the alternating signed v regions is likely coincident with a large scalar gradient. Accurately modeling this large scalar gradient as a function of the velocity field is a subject of future work. Additionally, from the work of Antonia *et al.* (2009) one can hypothesize that the structure of the temperature field may be similar to some combination of the streamwise and wall-normal velocity fields identified in this work. Future work aims to create a model of the scalar field that is compatible with the velocity field model of figure 5 to shed light on the instantaneous structural relationships between the two fields.

ACKNOWLEDGEMENTS

The authors would like to acknowledge the support of the Air Force, which made this work possible through a National Defense Science and Engineering Graduate Fellowship and two grants overseen by Doug Smith, #FA9550-12-1-0060 and #FA9550-16-1-0361. Additionally, the authors thank Dr. Scott Dawson for his assistance with the resolvent code in the boundary layer geometry.

REFERENCES

Antonia, R. A., Abe, H. & Kawamura, H. 2009 Analogy between velocity and scalar fields in a turbulent channel flow. *Journal of Fluid Mechanics* **628** (241-268).

Chen, C. H. P. & Blackwelder, R. F. 1978 Large-scale motion in a turbulent boundary layer: a study using temperature contamination. *Journal of Fluid Mechanics* **89** (1), 1–31.

DeGraaff, D. B. & Eaton, J. K. 2000 Reynolds-number scaling of the flat-plate turbulent boundary layer. *Journal of Fluid Mechanics* **422**, 319–346.

Gordeyev, S., Smith, A., Cress, J. & Jumper, E. 2014 Experimental studies of aero-optical properties of subsonic turbulent boundary layers. *Journal of Fluid Mechanics* **740**, 214–253.

Gordeyev, S., Smith, A. E., McKeon, B. J. & Saxton-Fox, T. 2015 Studies of the large-scale structure in adiabatic and moderately-wall-heated subsonic boundary layers. *The Proceedings of the Symposium on Turbulentce and Shear Flow Phenomena* **9**.

Hutchins, N. & Marusic, I. 2007 Large-scale influences in near-wall turbulence. *Philosophical Transactions of The Royal Society A* **365**, 647–664.

Jacobi, I. & McKeon, B. J. 2011 Dynamic roughness perturbation of a turbulent boundary layer. *Journal of Fluid Mechanics* **688**, 258–296.

Jacobi, I. & McKeon, B. J. 2013 Phase relationships between large and small scales in the turbulent boundary layer. *Experiments in Fluids* **54** (1481).

Kovasznay, L. S. G., Kibens, V. & Blackwelder, R. F. 1970 Large-scale motion in the intermittent region of a turbulent boundary layer. *Journal of Fluid Mechanics* **41** (2), 283–325.

Malley, M., Sutton, G. & Kincheloe, N. 1992 Beam-jitter measurements of turbulent aero-optical path differences. *Applied Optics* **31** (22), 4440–4443.

Mathis, R., Hutchins, N. & Marusic, I. 2009 Large-scale amplitude modulation of the small-scale structures in turbulent boundary layers. *Journal of Fluid Mechanics* **638**, 311–337.

McKeon, B. J. & Sharma, A. S. 2010 A critical-layer framework for turbulent pipe flow. *Journal of Fluid Mechanics* **658**, 336–382.

Monty, J. P., Hutchins, N., Ng, H. C. H., Marusic, I. & Chong, M. S. 2009 A comparison of turbulent pipe, channel and boundary layer flows. *Journal of Fluid Mechanics* **632**, 431–442.

Saxton-Fox, T., McKeon, B. J., Gordeyev, S. & Smith, A. E. 2015 Aero-optical distortion as a marker of turbulent structure. *The Proceedings of the International Symposium on Particle Image Velocimetry* **11**.

Wyckham, C. & Smits, A. 2009 Aero-optic distortion in transonic and hypersonic turbulent boundary layers. *AIAA Journal* **47** (9).

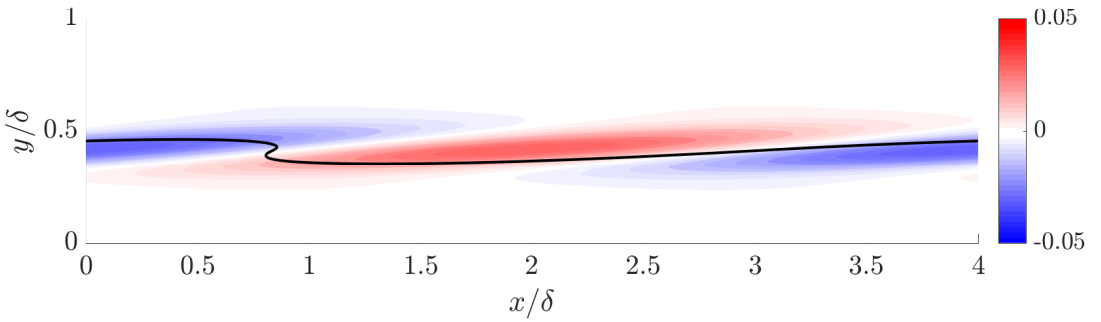

(a)

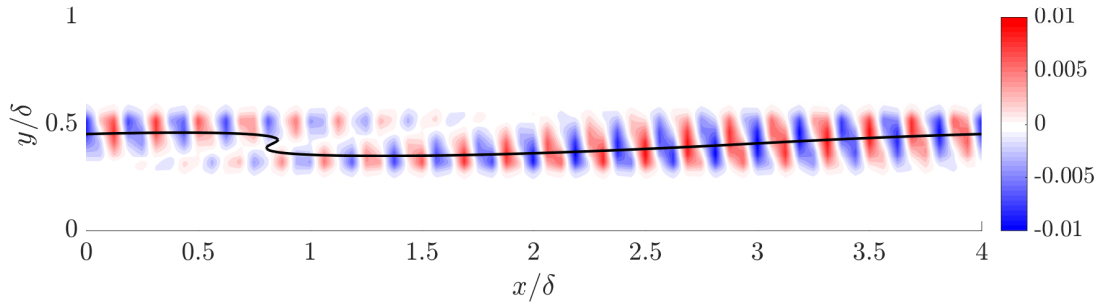

(b)

Figure 5: The interaction of the large and small scale velocity structure, shown in figure 4b, is modeled using eleven resolvent modes. The model of the large scale streamwise velocity mode is shown in (a) for reference. (b) represents the superposition of ten small scale wall-normal resolvent modes, with phases set from amplitude modulation statistics (Mathis *et al.*, 2009).The black line indicates $u+\bar{U}=0.8U_\infty$ where u is the fluctuating streamwise velocity field shown in (a). Note that $0.8U_\infty$ is the phase speed of the mode shown in (a).